A Novel RFID Based Pose Estimation Using Single Stationary Antenna

Samer S. Saab, *Senior Member*, *IEEE*, Hamze Msheik

***Abstract*—In this paper we propose a novel RFID based methodology that can estimate the position and orientation of an object. Unlike other RFID based localization systems, the proposed method employs a single non-steered stationary antenna and three passive tags mounted on each object. Our scheme is based on power map matching algorithm that is capable in estimating the location and orientation of objects. Unlike conventional power map matching schemes, which create the map from actual measurements, the proposed power map is automatically generated based on a simple mathematical model. The application under consideration is based on two-dimensional open spatial environment where the area of each object is no less than a quarter of a square meter with position estimation errors stretching to tens of centimeters. This work provides an alternative and relatively cheap approach for remotely estimating the pose of an object. As a proof of concept, we justify our scheme analytically and provide numerical and experimental data to substantiate the feasibility of our methodology.**

***Index Terms*— RFID, pose estimation, localization, power map matching, RSS, random shadowing error, quantizing errors**

I. Introduction

The first recorded use for RFID was World War II and was used to identify a friendly aircraft from foe [1]. The modern day use of RFID was first unveiled in Norway in 1987 where it was used as a toll collection tool [2]. The RFID business was estimated to be about 7.88$ billion dollar industry in 2013 and expected to grow to a staggering 30.24 billion in 2024 [3]. Accurate localization of assets using RFID technology is another desired application. Simply based on RFID range limitation, the reader can detect item proximity but not its exact location. Within the past decade, numerous and diverse proposed methodologies are published in the literature that come with a number of unique features. Different techniques are studied using Time of Arrival [4], Angle of Arrival [5], time difference of arrival [6], and phase difference of arrival [7]-[9]. A scheme is proposed combining software-based radio with accurate sampling of clocks used in conjunction with two antennas [5]. The scheme was tested in ideal conditions and never under real life conditions. TOA schemes impose a great additional cost for timing circuits and accurate sampling. In a highly dense passive tag distribution spatial domain, a localization algorithm [10] is proposed for mobile robot application resulting in localization accuracy of 10 cm. Based on experimental results evaluated in a straight line trajectory employing the algorithm in [10], a sparse tag distribution strategy is proposed [11] showing that the localization precision depends on the tag distribution density.

Manuscript received July 2, 2015; revised August 18, 2015; accepted September 18, 2015.

S. Saab is with the Department of Electrical and Computer Engineering, Lebanese American University, Lebanon, (email: ssaab@lau.edu.lb). H. Msheik was with the Department of Electrical and Computer Engineering, Lebanese American University, Lebanon (email: msheikhamze@gmail.com)

Similar performance is achieved with low tag distribution fused with odometry data [12]. An improved high-frequency RFID system using a sparse grid of floor tags coupled with a wheel encoder is proposed [13] for positioning and orientation of a moving object with accuracy of few centimetres. Another approach is based on the utilization of Received Signal Strength Indication (RSSI). The distance between transmitter and receiver can be estimated by studying the attenuation of the transmitted signal. However, the estimates are sensitive to radiation patterns of the antennas and multipath and shadowing effects. Based on the knowledge of the authors, the first published work employing RSSI attenuation model for standalone RFID-based localization system was proposed in [14]. Using mobile platforms and RSSI [14] and [15] the authors developed a reader-based RSSI localization scheme coupled with Kalman filter. The proposed scheme measured the RSS from nearby tags and was able to attain localization accuracy of about 12 cm [15]. Based on tag interaction analysis the k-nearest neighbour algorithm [16] and the simplex algorithm [17] are shown to have superior performance among other RSSI tag-based localization algorithms [17]. In [18], the authors developed a probabilistic sensor model based on the tag's RSSI measurement, the antenna orientation, and tag location. A rover would patrol the environment automatically creating a power lookup table. The process was repeated while adding different weight to values received. Using this scheme they were able to achieve an average of 29 cm accuracy in about 10 bootstrapping iterations. This approach requires a long calibration time rendering it unsuited for rapid deployment. Another proposed method fused information from ultrasonic sensors with RSS reading [19]. The scheme would use the RSS to obtain a rough estimate of location. The ultrasonic sensors information would be then fused with RSS data to improve localization to a couple of centimetres accuracy at short distances but with the additional cost of the ultrasonic sensors. Many others have worked on localization problem by mounting a reader on board an object [20]-[22]. While leading to a number of unique features, unlike tag-based applications, the reader-based schemes may not be cost effective or practical solution for various applications. Mounting a reader, antenna and a power supply on objects renders real life application infeasible due to cost. Based on the principles of radar systems, accuracy down to few centimetres is obtained when using electronically beam steered antenna [23]. However, none of the proposed RFID based systems estimate the position and orientation (or pose) of objects without mounting an antenna and its peripherals on the object itself. Pose estimation of an object remains a challenging problem addressed in the robotics community for object grasping and manipulation (e.g., see [24] and the references therein) and for estimating the poses of the robot (e.g., see [24]-[29]). Another class of applications includes assisted navigation, safety, and situation awareness in industrial areas [30]. The development of cost-efficient sensors has been one of the important topics in the field. Commonly used sensors for pose estimation are monocular

and stereo cameras and laser scanners. Accurate calibration and configuration of such sensors and luminance of the environment are crucial to the robustness of the associated pose estimation schemes. In addition, the algorithms that process them usually yield slow update rates.

Motivated by the aforementioned drawbacks this paper proposes a novel and cheap approach to pose estimation using passive RFID tag-based system. In particular, the proposed system setup employs a single non-steered beam stationary antenna with a reader, and it deploys three passive tags mounted on an object. The proposed pose estimation approach may not be well suited for general mass retailing application. However, typical applications could relate to robotics where object grasping and manipulation is considered including heavy autonomous forklift truck. The proposed pose estimation algorithm is based on power-map matching. The development of the power map is based on a logarithmic path loss model with an angle-dependent loss function. Error analysis due to random shadowing effects, reader power quantizing errors, and map quantizing errors are presented. A key performance variable associated with the proposed system is the distance that separates the tags that are mounted on the object. This paper also provides a formulation for tag separation that is based on statistical information of the various error sources. In addition, a robustification measure is presented that overcomes large measurement random errors. The application under consideration is based on two-dimensional open spatial environment where the area of each object is no less than a quarter of a square meter with position estimation errors in the order to tens of centimetres. Numerical and experimental results are presented in order to illustrate the feasibility of the proposed pose estimation system and to justify the analytical study presented in this paper. The main contributions of the proposed system are as follows:

- It provides an alternative methodology for remotely estimating the pose of an object.
- Unlike tag-based localization schemes, which either use multiple stationary antennas or beam steered antenna, the proposed system utilizes a single non-steered beam stationary antenna.
- The proposed system is designed not only to estimate the position of an object but also its orientation.
- Unlike conventional power map matching schemes, which create the map from actual measurements, the employed power map is generated based on a mathematical model.

This work may be considered to serve as a proof of concept of the proposed pose estimation system.

The rest of the paper is organized as follows. Section II states the problem under consideration with the system setup, and the concept behind the proposed approach. The development of the power map is also included in Section II. Error analyses are included in Section III. Section IV presents a formulation for the tag separation on an object and the power map matching algorithm. In Section V and VI, numerical and experimental results are included, respectively. Comparative characteristics of different pose estimation methods are presented in Section VII. Finally, we conclude and propose relevant future work in Section VIII.

II. Proposed Scheme

This section formally presents the statement of problem and system setup under consideration. It also includes the main concept of the proposed localization and orientation scheme, employed RSS model, and the development of the power map.

A. System Setup

The system is composed of a reader and one fixed antenna, and few passive tags placed on each object as depicted in Fig. 1. Fig. 1 is a snapshot in the lateral plane representing one scenario where four passive tags are placed on an object in a way they do not obstruct the line of sight with the antenna. The antenna could have been placed above or below the objects such that a line of sight is cleared between antenna and all tags and the tags are within the antenna range and beamwidth.

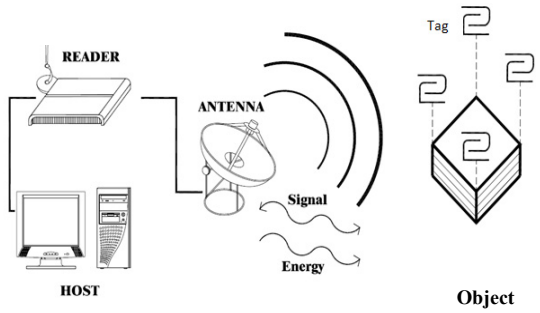

Fig. 1. Illustration of proposed system setup

B. Problem Statement

The problem is based on the following assumptions:

(A1). The coordinates of the stationary antenna are known

(A2). The position of each tag mounted on each object within the object frame is known. However, the position and orientation of the object are unknown.

(A3). The object is within the reader's operational range, within antenna major radiation lobe, and placed in the line of sight of antenna.

(A4). The radiation pattern of the tags possesses the characteristics of an omnidirectional antenna, which radiates radio wave power uniformly in all directions in the two-dimensional spatial domain under consideration.

Based on assumptions (A1)-(A4), develop an algorithm estimating the coordinates and orientation of an object that is only based on RSSI measurements.

C. Concept of proposed scheme

RSSI measures can be modelled as a nonlinear function of: 1) the distance between the antenna and object; 2) the object rotation angle; and 3) azimuth angle formed by the object and the antenna – assuming that tags are isotropic and their locations within the object frame are known. One RSSI measure results in one equation with three unknowns. Consequently, at least three tags placed at different locations on the object are required to estimate the position of the object. However, due to errors in RSSI measurements, deployment of more than three tags should improve instantaneous localization estimates. Directly solving such nonlinear equations in presence of measurement errors may lead to

infinite solutions. Another approach to the localization problem is by indirectly solving such nonlinear equations. In particular, a grid-like power map in the range of the antenna is generated using the pertinent nonlinear functions, and the RSSI measurements are simultaneously matched to their closest corresponding values. This approach can be considered as quantizing the solutions hence limiting the number of solutions. The latter approach is adopted in this manuscript and detailed in the subsequent sections.

D. Power Level Model

The adopted measured signal level model is based on the average received signal decreasing logarithmically with distance with log-normal shadowing. In particular, at a specific distance separation between antenna and tag, *d*, the measured signal levels (or RSSI) in dBm units, $P_r(d)$, have a Gaussian distribution about the path loss distance-dependent mean. At this point, we assume that the received power, $P_r(d)$, is in the direction of the strongest emission. Consequently, the signal level model is given by [15]

$$P_r(d)[dBm] = P_t[dBm] - PL(d) \quad (1)$$

$$PL(d) = \mathrm{E}[PL(d_0)] + 10q\log\left(\frac{d}{d_0}\right) + X_\sigma \quad (2)$$

where E[.] is the expectation operator, P_t is the tag transmitted backscattered power, $PL(.)$ is the average large-scale path loss, d_0 is the close-in reference distance, q is the path loss exponent, and X_σ, representing the random shadowing errors, is a zero-mean white Gaussian random variable in dB with standard deviation σ also in dB. The above model assumes that the antenna and tag are oriented such that the peak of radiation pattern of each antenna points in the direction of the other. In this manuscript, we assume that the antenna and the tags are placed on the same plane and that the radiation pattern of the tags has a "donut" shape, which practically make the tags as isotropic radiators. In practice the tags may be placed a bit lower than the antenna and in antenna's farfield. The latter is mainly due to antenna's relatively large beamwidth and the size of passive tags being relatively small. Usually a rough surface of an object can result in distorting the radiation pattern of a radiator. However, based on experimental results, such distortion may be considered insignificant due to the inherent and significant irregularities in the radiation pattern of such "cheap" RFID radiators. Another representation of the signal level model incorporating the antenna path loss is given by

$$P_r(d,\varphi) = P_r(d_0) - 10q\log_{10}\left(\frac{d}{d_0}\right) + L_D(\varphi) + X_\sigma \quad (3)$$

where $P_r(d_0) = P_t - E[PL(d_0)]$, φ is the angle that the tag makes with the main radiation beam of the antenna, and $L_D(\varphi)$ is the corresponding antenna angle-dependent loss.

E. Power Map Development

The proposed scheme relies on power map matching. The proposed method simulates RSS based on radiation pattern specific to the proximity of the employed antenna and tags. Based on the proposed localization system, it is essential to take full advantage of the geometric constraint resulting from the knowledge of the tags location with respect to the object frame while performing power map matching. A key feature of the proposed power map is in embedding the specific geometric constraint while constructing the power map.

The employed power map or lookup table is based on the following parameters: $P_r(d_0)$, d_0, q and radiation pattern, keyed into the following equation:

$$P_r(d_i,\varphi_i)[dB] = P_r(d_0) - 10q\log_{10}\left(\frac{d_i}{d_0}\right) + L_D(\varphi_i) \quad (4)$$

where d_i is the corresponding distance between the antenna and the i^{th} tag; d_0 is the reference distance with $L_D(0) = 0dB$; and φ_i is the angle that i^{th} tag makes with the main radiation beam of the antenna. The lookup table consists of three dimensions or variables. The first dimension refers to the distance between the antenna and the tag bounded by the farfield start (d_{min}) and sensitivity of reader and antenna deployed (d_{max}). The second dimension is the angle, φ, a tag makes with the main radiation beam of the antenna. φ is bounded by $\pm\pi$ for antennas with circular radiation pattern. However, directive antenna should be bounded by the main radiation lobe width (φ_{max}) due to side lobe irregularities rendering farfield power calculation inaccurate. The third dimension, θ, is the pivot of object around a specific point on the object. In particular, the object is represented by the *M* vertices of a fixed polygon representing the exact deployed locations of the tags with respect to object. The latter dimension covers our geometric constraint. Without loss of generality, we choose the point corresponding to Tag 1 as the pivoting point. The map variables are illustrated by the schematic below for *M* = 3.

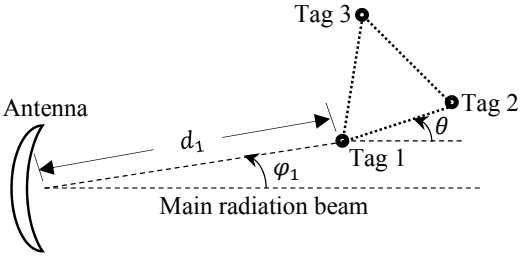

Fig. 2. Illustration of map variables

The following pseudo-code illustrates the off-line generation of the lookup table:

for ($d = d_{min}$; $d \le d_{max}$; $d = d + \Delta d$)
  for ($\varphi = \varphi_{min}$; $\varphi \le \varphi_{max}$; $\varphi = \varphi + \Delta\varphi$)
    for ($\theta = 0$; $\theta < 2\pi$; $\theta = \theta + \Delta\theta$)
      1. calculate the locations of corresponding points with respect to *d*, φ and Θ
      2. calculate RSS for each point using Equation (4).
      3. save into *M* tables and location indexed by *d*, φ and Θ. Each table represents a tag.

end; end; end.

where $\Delta d = \frac{d_{max} - d_{min}}{Q}$,$\Delta\varphi = \frac{\varphi_{max}}{Q}$, $\Delta\theta = \frac{2\pi}{Q}$, and Q is the number of special quantizing levels. The choice of Q is elaborated in subsection III- C below.

III. Error Analysis

In this section, the errors due to random shadowing effects, power quantization and map quantization are studied. Modelling errors due to the angle-dependent loss, $L_D(\varphi)$, can be as significant as random shadowing effects when

employing a directional antenna. The proposed algorithm limits the range of the radiation pattern of the antenna to its main radiation lobe. $L_D(\varphi)$ should be accurately modelled. Since resulting errors depend on an analytical model or lookup table, such errors are not thoroughly elaborated in the analytical part of this manuscript.

A. Random Shadowing Error

As described by the term X_σ (2), random shadowing effects (RSE) can result in a significant source of errors when estimating the distance between the tag and antenna. We denote such distance errors (resulting from X_σ) by δd_σ^{RSE}. It can be shown that the mean and standard deviation of δd_σ^{RSE} are given by [15]:

$$E[\delta d_\sigma^{RSE}(d)] = d(\mu - 1) \quad (5)$$

$$std[\delta d_\sigma^{RSE}(d)] = d\mu\sqrt{\mu^2 - 1} \quad (6)$$

where $\mu \triangleq exp\left[\frac{1}{2}\left(\frac{\ln(10)}{10q}\sigma\right)^2\right]$ and $d_0 \le d \le d_{max}$. We define

$$\Delta d_\sigma^{RSE} \triangleq E[\delta d_\sigma^{RSE}(d_{max})] + std[\delta d_\sigma^{RSE}(d_{max})] \quad (7)$$

Δd_σ^{RSE} is considered as a statistical bound representing RSE. Δd_σ^{RSE} grows proportionally to d_{max}. However, the corresponding proportionality constant decreases almost linearly for smaller values of σ.

B. Power Quantization Error

Most off-the-shelf RFID readers currently employ at least one processor to satisfy application requirements. Typically, a signal processor is interfaced to an analog-to-digital converter, which results in quantizing the outputs due to the limited range of the employed analog-to-digital converter. Most likely the signal is much larger than one least significant bit. Consequently, the quantization error is not significantly correlated with the signal, and has an approximately uniform distribution. This work assumes that the power quantizing error is a zero-mean uniformly distributed random variable.

Any actual received power variation, due to tag location variation, within two consecutive levels of measurements or reader's resolution, ΔP, is uncounted for. That is, variation in power below $\pm\Delta P/2$ will not induce a change in the reader's output. Therefore, due to its inability to properly represent the received power the reader itself will introduce an error, which we denote by Power Quantization Error (PQE). This section examines the maximum error resulting from PQE.

It is worthwhile mentioning that if the proposed system deployed only one tag, then this problem could not be properly resolved in two spatial dimensions due to singularities. In particular, there could be different tag locations corresponding to a fixed RSSI. Because the received power decreases logarithmically with distance, then the furthest tag locations within the vicinity of the antenna are considered most sensitive to PQE. Due to the directivity of the antenna, the furthest locations correspond to the minimum RSSI, P_{min}, the reader can sense whenever $\varphi \cong 0$. Therefore, the corresponding maximum distance between tag and antenna, satisfying $P_{min} = P_r(d_0) - 10q\log_{10}\left(\frac{d_{max}}{d_0}\right)$ is given by:

$$d_{max} \cong d_0 10^{\frac{P_r(d_0) - P_{min}}{10q}}.$$

The neighbourhood of that maximum location, corresponding to RSSI within $P_{min} - \Delta P/2$, are mapped to a single location due to PQE. The boundary of this neighbourhood can be considered as a circle with a radius Δd_{max}^{PQE} satisfying

$$P_{min} - \Delta P/2 = P_r(d_0) - 10q\log_{10}\left(\frac{d_{max} + \Delta d_{max}^{PQE}}{d_0}\right).$$

Therefore,

$$\Delta d_{max}^{PQE} = d_{max}\left(10^{\frac{\Delta P}{20q}} - 1\right) \quad (8)$$

C. Map Quantizing Error

The error resulting from quantizing the infinite number of points in continuous space to the finite discrete set of points created in our lookup table is called Map Quantizing Error (MQE). Increasing the planar sampling rate, Q, in the lookup table decreases the MQE. However, indefinite increase of Q will require indefinite computational throughput. This section describes MQE and provides means for selecting Q such that MQE becomes negligible with respect to PQE.

We first consider the case where the planar map is generated using two dimensions corresponding to Q_1 increments in distance radially away from antenna, Δd, and Q_2 increments in the azimuth angle that a point makes with main beam of the antenna, $\Delta\varphi$. If the *y*-axis is set along antenna main beam, then the error in the *y*-axis, δ_y, is bounded by $|\delta_y| \le \frac{d_{max} - d_{min}}{2Q_1}$, and the error in the *x*-axis, δ_x, is bounded by $|\delta_x| \le \frac{\varphi_{max}}{2Q_2} d_{max}$. If Q_1 and Q_2 are selected such that $\max|\delta_x| = \max|\delta_y|$, then we obtain $Q_1 = \frac{d_{max} - d_{min}}{d_{max}\varphi_{max}} Q_2$, which results in maximum two-dimensional Euclidean error corresponding to $\Delta d_{max}^{MQE} = \sqrt{2}\frac{\varphi_{max} d_{max}}{2Q_2}$. In order to have $\Delta d_{max}^{MQE} << \Delta d_{max}^{PQE}$; e.g., $10\Delta d_{max}^{MQE} = \Delta d_{max}^{PQE}$ then we set

$$Q_2 = round\left(\frac{5\sqrt{2}\varphi_{max}}{10^{\frac{\Delta P}{20q}} - 1}\right) \quad (9)$$

Consequently,

$$\Delta d_{max}^{MQE} \cong \frac{\left(10^{\frac{\Delta P}{20q}} - 1\right) d_{max}}{10} = \frac{\Delta d_{max}^{PQE}}{10} \quad (10)$$

IV. Map Matching Algorithm

This section includes a formulation for the mutual tag separation on an object and presents the proposed power map matching algorithm including a robustification measure.

A. Minimum Mutual Tags Separation

When the distance between the tags on an object is much smaller than the distance errors due to quantization and random shadowing, then the information contributed by deploying more than one tag per object would be lost by such random errors. This section examines the minimum mutual tags separation needed for effective tags placement.

Let d be the distance between antenna and a tag, and $d + \Delta D$ be the distance of another tag. Let φ_i be the angle that the i^{th} tag makes with the main radiation beam of the antenna. Since the study pertains to tag separation while considering the radiation pattern within the main lobe of a typical RFID reader antenna, we introduce the simplifying assumption that there exist two tags *i* and *j* among three tags mounted on an object

such that $L_D(\varphi_i) \cong L_D(\varphi_j) = L_D(\varphi)$. Therefore, the RSS corresponding to the two tags are given by:

$$P_r(d,\varphi) = P_r(d_0) - 10\,q\log_{10}\left(\frac{d}{d_0}\right) + L_D(\varphi) + X_{\sigma,n} + X_n^{PQE}$$

$$P_r(d+\Delta D,\varphi) = P_r(d_0) - 10\,q\log_{10}\left(\frac{d+\Delta D}{d_0}\right) + L_D(\varphi) + X_{\sigma,m} + X_m^{PQE}$$

where X_σ and X^{PQE} are the random variables representing RSE and PQE, respectively. In order to be able to have enough separation between the two RSS levels, we need the following inequality to be satisfied most of the times:

$$\Delta P_r \triangleq P_r(d,\varphi) - P_r(d+\Delta D,\varphi) > 0$$

$$\Delta P_r = 10\,q\log_{10}\left(\frac{d+\Delta D}{d}\right) + X_{\sigma,n} + X_n^{PQE} - X_{\sigma,m} - X_m^{PQE}$$

Therefore,

$$\Delta D > d(\rho\gamma_n\gamma_m - 1)$$

where $\rho \triangleq 10^{\frac{X_{\sigma,n}-X_{\sigma,m}}{10q}}, \gamma_n \triangleq 10^{\frac{X_n^{PQE}}{10q}}, \gamma_m \triangleq 10^{\frac{-X_m^{PQE}}{10q}}$, or $\rho = exp\left(\frac{\ln(10)}{10q}\left(X_{\sigma,n} - X_{\sigma,m}\right)\right), \gamma_n = exp\left(\frac{\ln(10)}{10q}X_n^{PQE}\right)$

$X_{\sigma,n}$ and $X_{\sigma,m}$ are identically distributed, therefore, $\left(X_{\sigma,n} - X_{\sigma,m}\right)$ is a zero-mean Gaussian random variable with $std\left(X_{\sigma,n} - X_{\sigma,m}\right) = \sqrt{2}\sigma$. However, the terms (ρ,γ_n,γ_m) in the above inequality need further elaboration for establishing a lower bound forΔD. Let $\xi(d) \triangleq d(\rho\gamma_n\gamma_m - 1)$. It is worth noting that X_n^{PQE} and X_m^{PQE} are due PQE corresponding to two different points in space, hence statistically independent. Furthermore, X_σ is due to RSE, which is independent of PQE. Therefore, ρ, γ_n, and γ_m are independent random variables, and γ_n and γ_m are identically distributed. Thus,

$$E(\xi(d)) = d(E(\rho)E^2(\gamma_n) - 1)$$

$$std(\xi(d)) = d\sqrt{E(\rho^2)E^2(\gamma_n^2) - E^2(\rho)E^4(\gamma_n)}$$

where, it can be shown that,

$$E(\rho^j) = exp\left[\left(\frac{j\ln(10)}{10q}\right)^2\sigma^2\right], j \in \{1,2\} \quad (11)$$

$$E\left(\gamma_n^j\right) = \frac{1}{\Delta P}\int_{-\frac{\Delta P}{2}}^{\frac{\Delta P}{2}} exp^j\left(\frac{\ln(10)}{10q}x\right)dx, j \in \{1,2\} \quad (12)$$

Consequently, for effective multiple-tag deployment on an object, the mutual tags separation, $\overline{\Delta D}$, within the object is recommended to be around $(E(\xi(d)) + std(\xi(d)))|_{d=d_{max}}$ so that the probability of $\Delta D < d(\rho\gamma_n\gamma_m - 1)$ becomes negligible for all d. That is,

$$\overline{\Delta D} \cong d_{max}f(\sigma,q,\Delta P) \quad (13)$$

where

$$f(\sigma,q,\Delta P) = E(\rho)E^2(\gamma_n) - 1 + \sqrt{E(\rho^2)E^2(\gamma_n^2) - E^2(\rho)E^4(\gamma_n)}$$

$E(\rho^j)$ and $E\left(\gamma_n^j\right), j \in \{1,2\}$ are obtained from (11) and (12).

In general, larger separation would provide more robust information and higher localization accuracy. However, the larger associated space required would render the application efficiency of the proposed system taking into consideration the limited range of the antenna coverage.

Remark 1: For $0.1 \le \sigma \le 2, 2 \le q \le 4,$ and $0 \le \Delta P \le 1$, an approximation of the tag separation is given by, $\overline{\Delta D} \cong d_{max}\frac{3}{10q-5}\sigma$. The latter indicates that $\overline{\Delta D}$ is dominated by RSE and is proportional to σ. In what follows, we refer to the sampling rate of a reader to be the ability of a reader acquiring a number of RSS measurements per second. The effects of random shadowing on $\overline{\Delta D}$ can be reduced when employing a moving average on the power meaurements provided that: a) several measures can be taken in a small time interval at the same position, and b) X_σ, representing RSE, is a zero-mean white Gaussian random variable in dB (with standard deviation σ).The latter assumption comes with limitation since at arbitrary large sampling rates, the correlation between power samples may become significant, that is, X_σ may no longer be assumed white. In particular, the filtered measured power at time instant, k, is given by $\bar{p}_k = \frac{1}{N}\sum_{k-N+1}^{k} p_i$, where p_i is the measured power at instant i. It is assumed that within N samples, the tag is stationary. If we let $\bar{X}_\sigma$ represent the random shadowing associated with $\bar{p}_k$, then it can be shown that $\bar{X}_\sigma$ is also a zero-mean Gaussian random variable with standard deviation $\sigma/\sqrt{N}$. Thus, employing a reader with a sampling rate of 10^{2n}Hz and a moving average with width = 1 sec, decreases the standard deviation of $\bar{X}_\sigma$ by 10^n, and consequently, $\overline{\Delta D}$ decreases by n orders of magnitude. For example, using one-second moving average with sampling rate of 100Hz, $\sigma = 1.2$, $q = 4$ and $d_{max} = 100$ m, then $\overline{\Delta D} \cong$ 1m.

Remark 2. When modelling errors due to the angle-dependent loss, $L_D(\varphi)$, are significant, it can be shown that

$$\Delta D = d(\rho\gamma_n\gamma_m\lambda_n\lambda_m - 1)$$

where $\lambda_n = [l_D(\varphi_n)]^{1/q}$ and $L_D(\varphi) = 10\log_{10}\left(l_D(\varphi)\right)$. In addition, if φ is assumed to be uniformly distributed over $\varphi_1 \le \varphi \le \varphi_2$, then $E[\lambda^j] = \frac{1}{\varphi_2-\varphi_1}\int_{\varphi_1}^{\varphi_2} l_D(\varphi)^{j/q}d\varphi, j \in \{1,2\}$. Since ρ, γ_n, and γ_m can be assumed independent random variables, then the mean and standard deviation of $\xi(d)$ become:

$$E(\xi(d)) = d(E(\rho)E^2(\gamma_n)E^2(\lambda_n) - 1)$$

$$std(\xi(d)) = d\sqrt{E(\rho^2)E^2(\gamma_n^2)E^2(\lambda_n^2) - E^2(\rho)E^4(\gamma_n)E^4(\lambda_n)}$$

B. Power Map Matching Algorithm

Instead of matching the RSS individually, the RSS of the M tags installed on an object are simultaneously compared with pre-stored sets of M simulated power values. These modelled power values, $p_{m,k}$ with $1 \le m \le M$ and $k = 1,2,\ldots$, satisfy the tag placement geometric constraint, where index k is the cell indicator in the lookup table. Each $p_{1,k}$ is associated and indexed to a triplet (d_k,φ_k,θ_k) as illustrated in Fig. 2. The object pose is described by (d_1,φ_1,θ) where (d_1,φ_1) are the polar coordinates of Tag 1. If $p_{j,k}$ turns out to be a valid match for a specific value of k, then the location of the object is determined by (d_k,φ_k) and its rotation by θ_k.

Based on the specific tags identification numbers corresponding to each object, the relevant RSS are first grouped. The M RSS readings, $\hat{p}_n$ with $1 \le n \le M$, are then sent to our match map locater. The match locator is a simple comparator. The power map matcher first identifies the best match and then check for its validity. The matching algorithm is based on the following measure:

$$\mathcal{E}(k) \triangleq \sqrt{\sum_{j=1}^{M}(p_{j,k} - \hat{p}_j)^2} \quad (14)$$

The best match corresponds to the minimum value of $\mathcal{E}(k)$. Let $\bar{\mathcal{E}} = \mathcal{E}(k=\kappa) = \min_k \mathcal{E}(k)$. Next, the algorithm checks for the validity of the obtained match due to the effects of large random variability. In particular,

If $\bar{\mathcal{E}} > C$, match is considered invalid
If $\bar{\mathcal{E}} \leq C$, match is considered valid

The choice of C can be relevant to the robustness of the algorithm. Basically for larger values of PQE, RSE and MQE, the value of C is made larger. Selection of C is subsequently elaborated. Let $\hat{p}_n$ be the measured power for a specific location *n* and let p_m be the simulated power for a location *m* on the power map nearest to location *n*. Consequently, $\hat{p}_n$ can be modelled as:

$$\hat{p}_n = P_r(d_0) - 10\,q\left(\frac{d_n}{d_0}\right) + L_D(\varphi_n) + X_{\sigma,n} + X_n^{PQE} \quad (15)$$

where $X_{\sigma,n}$ and X_n^{PQE} are the random variables representing RSE and PQE, respectively. On the other hand,

$$p_m = P_r(d_0) - 10q\log_{10}\left(\frac{d_m}{d_0}\right) + L_D(\varphi_m)$$

Since the *m* location on the map is nearest to location *n*, then the right hand term can be re-written as

$$p_m = P_r(d_0) - 10q\log_{10}\left(\frac{d_n}{d_0}\right) + L_D(\varphi_n) + X_m^{MQE}$$

where X_m^{MQE} is a random variable representing variation of power due to MQE. Therefore,

$$p_m - \hat{p}_n = X_m^{MQE} - X_{\sigma,n} - X_n^{PQE} \quad (16)$$

As described in Section III.B, the PQE is assumed to be a zero-mean uniformly distributed random variable. Therefore, X_n^{PQE}, representing power quantizing *errors*, is a zero-mean random variable uniformly distributed over $\pm\Delta P/2$. Since the map is sampled such that MQE << PQE, then MQE is neglected. Next we consider $\mathcal{E}(k)$ given in (14). Based on Monte Carlo simulations, the mean and standard deviation of $\mathcal{E}(k)$, where a match is assumed, can be closely approximated as follows for $3 \leq M \leq 10$:

$$E[\mathcal{E}(k)] \cong \sqrt{\mu_{\sigma,M}^2 + \mu_{PQE,M}^2} \quad (17)$$

$$std[\mathcal{E}(k)] \cong \sqrt{std_\sigma^2 + std_{PQE}^2} \quad (18)$$

where

$$\mu_{\sigma,M} \cong \sigma(M+5)/5 \qquad std_\sigma \cong 0.68\sigma$$
$$\mu_{PQE,M} \cong \Delta P(0.06M + 0.3) \qquad std_{PQE} \cong 0.136\Delta P$$

We choose C as follows:

$$C = E[\mathcal{E}(k)] + std[\mathcal{E}(k)] \quad (19)$$

Remark 3: It is worthwhile noting that the choice of C does not depend on the tag separation distance. For smaller values of C, robustness of the algorithm is improved but at the cost of a significant likelihood not to obtain a valid match at a specific sample. However, if at one sample a match turns out to be invalid for values of C as suggested in Equation (19), then more attempts are made for each item until a valid match is obtained.

Remark 4: Application can involve simultaneous localization of several objects. The processing involved in map matching can be demanding – an efficient technique to speed up the search process is desired. Instead of searching for a match within the entire power map domain, we confine the search domain to a significantly smaller domain using a starting point and two constraints. The starting point is obtained by finding the very first valid match. Inserting the simulated power of Tag 1, which corresponds to the starting point, in Equation (4) provides a line constraining possible ranges, d in relation with associated angles, φ. This line defines the curvature of the domain, almost shaped as the antenna's radiation pattern. The "width" of the new search domain is obtained by using the adopted match-validity constraint, $\sqrt{\sum_{j=1}^{M}(p_{j,k} - \hat{p}_j)^2} \leq C$. This process is repeated for all increments of θ.

V. Numerical Simulation Results

This section illustrates the performance of the proposed system due to RSE, PQE, path loss exponent, *n,* number of tags per object, M, and the spacing between tags, $\overline{\Delta D}$. MATLAB is employed for all numerical simulations.

A. Example 1.

This example illustrates the performance of various tag separations and the effect of deploying three and four tags per object. In order to illustrate the observation made in Remark 1, we also consider the effect of taking the RSS average of 100 measures over no RSS averaging (considering only one RSS sample) for each location, as suggested in Remark 1. PQE is not considered, $L_D(\varphi) = 2\times10^{-3}\varphi^2$ [dB] (φ in degrees), $q = 3$, and $\sigma = 1$. Objects are spread uniformly within a planar domain bounded by $100 \leq d \leq 1000$ cm and $0 \leq \varphi \leq 70^o$. The space is sampled using $Q = 100$ resulting in MQE bounded by $\pm$ 7.6 cm. Equation (13) suggests a tag separation of 120 cm. Fig. 3 shows the average of all localization absolute errors versus different tag separations ranging from 40 cm to 120 cm. Fig. 4 and Fig. 5 show the cumulative distributions of the absolute errors corresponding to position and orientation, respectively, for a tag separation of 80 cm.

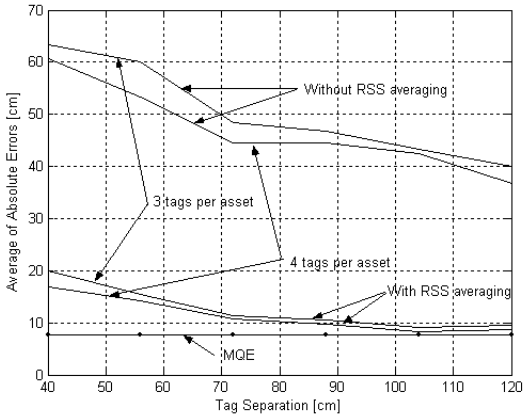

Fig. 3. Mean absolute errors versus tag separation

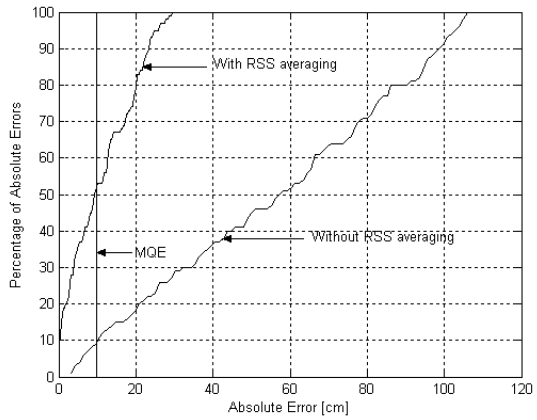

Fig. 4. Cumulative distribution of position errors for the case of three-tag deployment and with tag separation = 80 cm

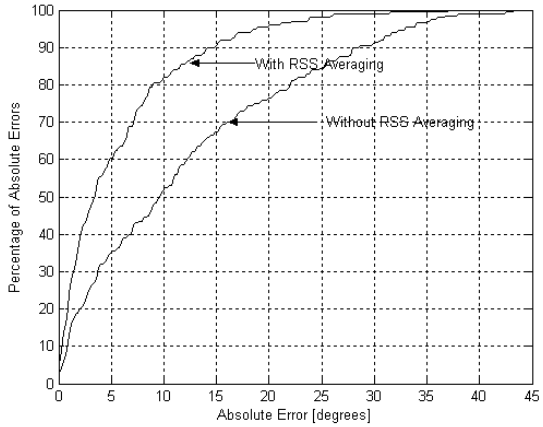

Fig. 5. Cumulative distribution of orientation errors for the case of three-tag deployment and with tag separation = 80 cm

The following conclusions can be drawn from simulations:

- The improvement in using four-tag deployment over three tags per object is not that significant while taking into consideration that the area required for four-tag deployment may be twice as large.
- As expected, as the separation between tags increases, the error decreases.
- As shown in Figures 3-5, the position and orientation errors become significantly smaller when we average the RSS measurements. However, as indicated in Remark 1, averaging RSS measurements requires many samples at each position – a trade-off between precision and time spent to collect different samples. In addition, if the power sampling rate is increased, then the time spent to estimate a pose becomes smaller. However, arbitrary increasing the sampling rate would result in correlated power samples, which would eventually lead to saturated performance yielding a lower bound on these errors.
- Fig. 4 shows that 70% of the position errors are less than 80 cm (smaller than the size of the object) when no RSS averaging is employed, and 30% of the position errors are between 80 cm and 105 cm. In addition, 100% of the errors are smaller than 25 cm with RSS averaging.
- Fig. 5 shows that 70% of the orientation errors are less than 16 degrees when no RSS averaging is employed whereas 70% of the errors are smaller than 7 degrees when RSS averaging is employed.

It is worthwhile mentioning that, in order to include MQE, most of the exact locations of the objects do not perfectly match the locations associated with the map. Otherwise, the errors would become significantly smaller and in extreme cases where the tag separation is relatively large and σ is relatively small, then all errors become exactly zero.

B. Example 2

This example validates the analytical results provided in this manuscript. In particular, different values of $\sigma, q,$ and ΔP are considered where the choice of C, Q, and $\overline{\Delta D}$ are selected according to Equations (19), (9), and (13), respectively. The planar domain is similar to the one employed in Example 1. Since the effect of RSE is most significant, several values of σ are considered: $\sigma \in \{0.1, 0.2, \ldots, 2\}$. This study does not employ RSS averaging. The performance under consideration is first taking the average of absolute localization errors corresponding to each σ, q and ΔP, $\bar{E}_\sigma$, and then take average and standard deviation of $\bar{E}_\sigma$ among different values of σ. The performance is summarized and listed in Table 1 for two tag-deployment scenarios, $M = 3$ and $M = 4$. Table 2 and Table 3, corresponding to position errors and orientation errors, respectively, list the values of $\bar{E}_\sigma$ for $M = 3$ for different values of σ. Based on the recommended values of C, Q, and $\overline{\Delta D}$, one should expect compatible performance for different values of $\sigma, q,$ and ΔP.

TABLE 1. PERFORMANCE CONSISTENCY

		$q = 2.5$		$q = 3.5$	
		$\Delta P = 0.1$	$\Delta P = 1$	$\Delta P = 0.1$	$\Delta P = 1$
$M = 3$	Avg($\bar{E}_\sigma$)[1]	7.4cm	11.8cm	11cm	10.2cm
	Std($\bar{E}_\sigma$)[1]	1.3cm	0.6cm	1.2cm	0.9cm
$M = 4$	Avg($\bar{E}_\sigma$)[1]	6.9cm	11cm	9.8cm	8.9cm
	Std($\bar{E}_\sigma$)[1]	1.1cm	1cm	1.2cm	1.1cm

1. The values of Avg and Std represent the average and standard deviation for $\sigma \in \{0.1, 0.2, \ldots, 2\}$ pertaining to $\bar{E}_\sigma$.

TABLE 2. PERFORMANCE CONSISTENCY: POSITION WITH $M = 3$

		$q = 2.5$		$q = 3.5$	
		$\Delta P = 0.1$	$\Delta P = 1$	$\Delta P = 0.1$	$\Delta P = 1$
$\bar{E}_\sigma$	$\sigma = 0.5$	9.5cm	13.4cm	8.6cm	9.0cm
	$\sigma = 1.0$	7.1cm	10.7cm	10.6cm	9.6cm
	$\sigma = 1.5$	6.5cm	11.8cm	11.8cm	11.2cm
	$\sigma = 2.0$	6.0cm	12.0cm	11.7cm	10.9cm

TABLE 3. PERFORMANCE CONSISTENCY: ORIENTATION WITH $M = 3$ AND $\Delta P = 1$

		$q = 2.5$	$q = 3.5$
$\bar{E}_\sigma$	$\sigma = 0.5$	4.6 degrees	3.6 degrees
	$\sigma = 1.0$	4.0 degrees	3.7 degrees
	$\sigma = 1.5$	4.4 degrees	4.4 degrees
	$\sigma = 2.0$	4.3 degrees	3.8 degrees

The values listed in Tables 1-3 show that the relatively small variations among all pose errors. The average of localization errors ranges from about 7 cm to 12 cm and standard deviations $\approx$ 1 cm with orientation errors $\approx$ 4 degrees corresponding to the different values of $\sigma, q,$ and ΔP. The consistency among numerical results illustrates the validity of the analytical results.

Remark 5: All simulation results justify that the errors corresponding to object locations closer to antenna are smaller as reflected in (5), (6) and (8). Consequently, in applications where objects vary in dimension, then it becomes quite natural to place larger objects further from antenna in order to achieve more uniform localization accuracy. The latter assumes that larger objects inherit larger tag separation deployment.

VI. Experimental Results

Our proposed approach has been implemented and tested using the equipment listed in Table 4.

TABLE 4. EQUIPMENT UTILIZED

Reader (by Impinj Speedway)	Operating Frequencies	865-956 MHz
	RF Power	+30dBm
	Operating Temperature	-20 to 55°C
Antenna (by Laird Technologies)	Gain	12 dBi
	Polarization	LHCP
	Set Output Power	30 dBm
	Set Frequency	867 MHz
Tag[1]	ID	RSI-611

1. Allien Bat tags with size 8.5cm×3.5cm

Two classes of tag deployment are studied. In particular, for $M = 3$, the tags are installed at the vertices of a right isosceles triangle. Four different rotations of the triangular object are considered for each location: down, up, left and right. For $M = 4$, the tags are installed at the vertices of a square with area twice as large as of the triangle used for $M = 3$. The antenna and tags are placed at 1.8 m from the ground in an open space environment. The location of antenna and distribution of objects, for both scenarios $M = 3$ and $M = 4$, are illustrated in Fig. 6. It is worthwhile noting that each position of the object is changed and then its pose is estimated.

The main lobe of the employed antenna is about $\pm 50^o$. The employed model for the angle-dependent path loss is given by:

$$L_D(\varphi) = \begin{cases} 0, & |\varphi| \le 30^o \\ 2.2 \times 10^{-3}\varphi^2 & |\varphi| > 30^o \end{cases}.$$

The reader's resolution $\Delta P = 1$ dB, and the path loss exponent $q \approx 2$ with associated $\sigma \lesssim 1$. The range of the antenna $d_{max} \approx 3.5$ m. According to Equations (9), (13), and (19), the number of quantizing levels $Q \approx 105$, the match-validity threshold $C = 2.33$ for $M = 3$ and $C = 2.57$ for $M = 4$, and mutual tag separation on an object should be $\overline{\Delta D} \gtrsim 70$ cm. However, we choose $Q = 100$ and two different tag separations of 40 cm and 80 cm.

Table 5 lists the localization and orientation absolute errors, whereas Fig. 7 and Fig. 8 show the cumulative distribution (CD) of errors. It can be concluded that:

- For $M = 3$ and tag spacing of 40cm, 90% of the absolute errors are less than 100cm (distance) and 25° (rotation), and for tag spacing of 80cm, 90% of the absolute errors are less than 50cm (distance) and 14° (rotation).
- The performance improvement when using $M = 4$ over $M = 3$ is more significant at the smaller tag spacing.
- The localization and orientation errors are smaller when tags are closer to the antenna.

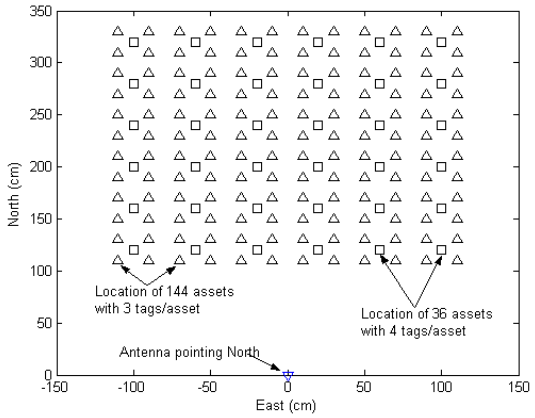

Fig. 6. Location of antenna and distribution of objects with tag separation = 40 cm

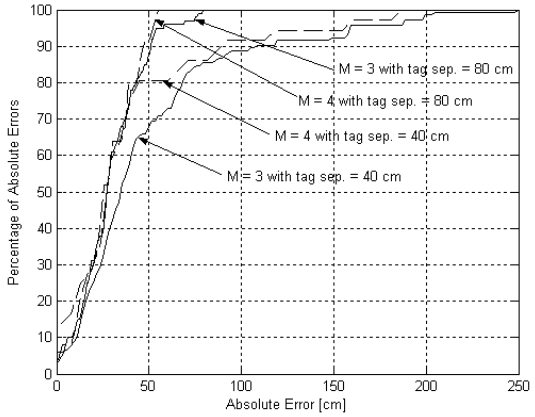

Fig. 7. CD of *position* errors for the case of three- and four-tag deployment with tag separation equal to 40 cm and 80 cm

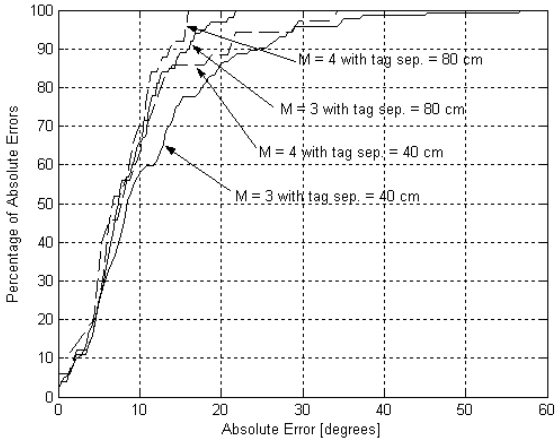

Fig. 8. CD of *orientation* errors for the case of three- and four-tag deployment with tag separation equal to 40 cm and 80 cm

TABLE 5. STATISTICAL VALUES OF ABSOLUTE ERRORS

	Tag Sep. = 40cm		Tag Sep. = 80cm	
	$M = 3$	$M = 4$	$M = 3$	$M = 4$
Avg. dist.	50.14cm	40.91cm	29.34cm	28.1cm
Std. dist.	47.6cm	41.9cm	17.3cm	15.1cm
Max. dist.	250.7cm	188.9cm	79.6cm	55.9cm
Avg. Ang	11.7°	9.6°	8.5°	8°
Std. Ang.	9.3°	17.7	5°	4.3°
Max. Ang	57°	34°	21°	16°

TABLE 6. CHARACTERISTICS OF POSE ESTIMATION METHODS

Method	a)	b)	c)	d)	e)	f)	g)
[25]	Several ultrasonic Txs attached to the ceiling. On board: 3 ultrasonic Rxs and odometers	2D	N	N	Y	L	Pos. ≤ 0.88m Orient. ≤ 52^o
[26]	On board: 6DOF Inertial Meas. Unit with magnetometers and position sensor	3D	N	Y	Y	H	Pos. ≤ 0.5mm Orien. ≤ 1.3^o
[27]	On board: 3 laser sensors, goinometers, IR camera, and harmonic geared motors	3D	Y	Y	N	H	Pos. < 1mm Orien. < 1^o
[28]	On board: Anisotropic magnetoresistive sensors, and sonar sensors	2D	N	N	N	≈L	Pos. ≈5cm Orient. ≈ 10^o
[29]	On board: A sensor-based servoing range senor (Kinect)	3D	Y	Y	Y	H	Pos. ≈3mm Orient. ≈ 0.4^o
[30]	Surveillance camera and an off-board thermal camera	2D	N	Y	Y	H	Pos. ≈0.75m Orient. ≈ 6.7^o
Our method	One RFID reader and 3 passive tags/object	2D	N	N	N	L	Pos. ≤ 0.5m Orien. < 12^o

Comparative Discussion on Pose Estimation

This section compares selected recent findings [25]-[30] on pose estimation with our proposed approach. The comparison is based on the following criteria:

a) Required sensors
b) Spatial dimensions: (2D or 3D)
c) Luminance constraint: Yes or No (Y/N)
d) Calibration requirement: Yes or No (Y/N)
e) Initialization requirement: Yes or No (Y/N)
f) Update rates: L (if less than 1ms) or H (of more than 1 s)
g) Accuracy: Mean of position and orientation errors (based on experimental results and specific application)

The results are summarized in Table 6. All proposed methods in [25]-[30] come with a number of unique features and constraints. Although the precision of our proposed method can be considered inferior to most, it comes with several significant advantages. In particular, it provides a cheap and novel solution with relatively fast update rates, and it does not require luminance, calibration, or initialization.

Remark 6: Based on the experimental results, the errors can be decreased to:

- 0.41m and 9.6^o when 4 tags are deployed instead of 3 with 0.4m tag separation (Table 5).
- 0.29m and 8.5^o when the tag separation is 0.8m with 3 tags are deployed (Table 5).

The employed reader by Imping is not designed for localization/pose application (e.g., PQE is 1 dB). Consequently, an adequate reader should result in smaller errors. In addition, the accuracy depends on the type of application under consideration. For example, consider an application of a heavy (e.g., 20 tons) autonomous forklift truck where an adequate reader and omnidirectional antenna are installed on the truck. Such application comes with the following two key advantages:

1. The deployment of several tags can be spread along the object to be lifted with maximum tag separation of few meters. Consequently, the errors can be made significantly smaller. The latter is analysed in Section IV-A and illustrated in Fig. 3.
2. As the truck approaches the object the errors become smaller; e.g., see (5) and (6).

VII. Conclusion and Future Work

This paper presented a novel, cheap and simple approach for pose estimation using RFID technology. The proposed system employed only one non-steered beam stationary antenna with multiple tags installed on an object. The power map was developed using a model for RSS signals. Three passive tags were shown to be sufficient for localization. Analytical study supported by experimental and numerical simulations showed the feasibility of the proposed system in estimating the pose of an object. Numerical and experimental results showed that the localization and orientation errors can be made smaller by increasing the tag separation and/or to a lesser extent, deploying of four tags per object. Experimental results showed that the average of absolute errors ≈ 29 cm (distance) and 8.5^o (rotation) and 90% of the absolute errors are less than 50 cm (distance) and 14^o (rotation) for a tag separation of 80 cm only by deploying three tags per object and without using averaging of RSS measurements.

Two relevant issues that are worthwhile investigating that were not addressed in this manuscript: a) performance analysis of different objects with different materials and environments along with the effects of neighboring radiators; and b) application of the proposed approach to a three-dimensional localization setup. More work can be done to improve the performance of the proposed methodology: a) employment of a reader with significantly smaller power quantizing errors; and b) employment of an antenna with circular radiation pattern. In attempt to reduce the "minimum" needed tag separation, phase readings, possibly integrated with RSSI measurements, are worthwhile examining. In addition, experimental work can involve a study of pose estimation performance versus power sampling frequency while considering RSS averaging.

ACKNOWLEDGMENT

The authors would like to thank all eleven anonymous reviewers for their constructive suggestions in improving this work, and especial appreciation goes to Reviewer 4 for providing us with thorough comments and helpful suggestions. Special thanks go to Mr. Joe Khalife who helped us in conducting the experiments and simulations.

References

[1] R. C. Watson, Jr.; Radar origins worldwide: History of its evolution in 13 nations through World War II, Trafford Publishing, 2009.
[2] S. Lahiri, *RFID Sourcebook*: IBM Press, 2005.
[3] R. Das, P. Harrop, "RFID Forecasts, Players and Opportunities 2014-2024," London, 2013.
[4] H. Lee, D. W. Engels, R. Elmasri, J. S. Choi, "Passive UHF RFID

based localization using detection of tag interference on smart shelf," *IEEE Trans. Syst., Man, Cybern. C, Appl. Rev.*, pp. 268-275, Feb. 2012.

[5] S. Azzouzi, M. Cremer, U. Dettmar, R. Kronberger, and T. Knie, "New measurement results for the localization of UHF RFID transponders using an angle of arrival (AoA) approach," *in Proc. IEEE Int. Conf. RFID*, pp. 91–97, Apr. 12-14, 2011.

[6] Y. Huang, P. V. Brennan, and A. Seeds, "Active RFID location system based on time-difference measurement using a linear FM chirp tag signal," *in Proc. IEEE Int. Symp. Pers., Indoor Mobile Radio Commun*., pp. 1–5, Sep. 15-18, 2008.

[7] B. Grant, X. Liu, Z. Zhang, and P. Kumar C. Hekimian-Williams, "Accurate localization of RFID tags using phase difference," *IEEE Proc. of Int. Conf. on RFID*, vol. 1, no. 1, pp. 89-96, 2010.

[8] F. Martinelli E. DiGiampaolo, "Mobile robot localization using the phase of passive UHF-RFID signals," *IEEE Trans. Ind. Electron.*, pp. 365-376, Jan. 2014.

[9] C. Hekimian-Williams, B. Grant, X. Liu, Z. Zhang, and P. Kumar, "Accurate localization of RFID tags using phase difference," *in Proc. IEEE Int. Conf. RFID*, pp. 89–96, Apr. 14-16, 2010.

[10] S. S. Han, H. S. Lim, and J. M. Lee, "An efficient localization scheme for a differential-driving mobile robot based on RFID system," *IEEE Trans. Ind. Electron*., vol. 54, no. 6, pp. 3362–3369, Dec. 2007.

[11] P. Yang, W. Wu, M. Moniri, and C. C. Chibelushi, "Efficient object localization using sparsely distributed passive RFID tags," *IEEE Trans. Ind. Electron*., vol. 60, no. 12, pp. 5914-5923, Dec. 2013.

[12] E. DiGiampaolo, F. Martinelli, "A passive UHF-RFID system for the localization of an indoor autonomous vehicle," *IEEE Trans. Ind. Electron*., pp. 3961-3970, Oct. 2012.

[13] M. Y. Ahmad and A. S. Mohan, "Novel bridge-loop reader for positioning with HF RFID under sparse tag grid," *IEEE Trans. Ind. Electron*., vol. 61, no. 1, pp. 555-566, Jan. 2014

[14] S. S. Saab, W. Mhanna, S. Saliba, "Conceptualisation study of using RFID as a stand-alone vehicle positioning system," *Int. J. Radio Freq. Identification Techn.*, vol. 2, no. 1, pp. 27-45, 2009.

[15] S. S. Saab, Z. Nakad "A standalone RFID indoor positioning system using passive tags," *IEEE Trans. Ind. Electron.*, pp. 24-40, May 2011.

[16] L. M. Ni, Y. Liu, Y. C. Lau, and A. P. Patil, "LANDMARC: Indoor location sensing using active RFID," *Wireless Netw*., vol. 10, no. 6, pp. 701–710, Nov. 2004.

[17] Z. Zhang, Z. Lu, V. Saakian, X. Qin, Q. Chen, and L.-R. Zheng, "Item-Level Indoor localization with passive UHF RFID based on tag interaction analysis," *IEEE Trans. Ind. Electron*., vol. 61, no. 4, pp. 2122-2135, Apr. 2014.

[18] D. Joho, C. Plagemann, W. Burgard, "Modeling RFID signal strength and tag detection for Localization and mapping," in *IEEE Int. Conf. on Robotics and Auto.*, Kobe, Japan, May 12-17, 2009.

[19] B. S. Choi, J. J. Lee, "Mobile robot localization scheme based on RFID and sonar fusion system," *IEEE Proc. of Int. Symp. on Ind. Electron.*, pp. 1035-1404, Jul, 5-8, 2009.

[20] B.S. Choi, J. W. Lee, J. J. Lee, and K. T. Park, "A hierarchical algorithm for indoor mobile robot localization using RFID sensor fusion," *IEEE Trans. Ind. Electron.*, vol. 55, no. 6, pp. 2226-2235, Jun. 2011.

[21] S. Han, H.S. Lim, J.M. Lee," An efficient localization scheme for a differential-driving mobile robot based on RFID system," *IEEE Trans. Ind. Electron.*, pp. 3362-3369, Dec. 2007.

[22] S. Park, S. Hashimoto, "Autonomous mobile robot navigation using passive RFID in indoor environment," *IEEE Trans. Ind. Electron.*, vol. 56, no. 7, pp. 2366-2373, Jul. 2009.

[23] A. Bouzakis, L. Overmeyer, "RFID tag positioning with the aid of an active electronically-steered array," *IEEE Proc. of Int. Symp. on PIMRC*, pp. 2483-2488, Sep. 9-12, 2012.

[24] J. Bohg, A. Morales, T. Asfour, D. Kragic "Data-driven grasp synthesis—A survey," *IEEE Trans. Robot*., vol. 30, no. 2, pp. 289-308, Apr. 2014.

[25] S. J. Kim, B. K. Kim, "Dynamic Ultrasonic Hybrid Localization System for Indoor Mobile Robots," *IEEE Trans. Ind. Electron.*, vol. 60, no. 10, pp. 4562-4573, Oct. 2013.

[26] G. Du, P. Zhang, "Online Serial Manipulator Calibration Based on Multisensory Process Via Extended Kalman and Particle Filters," *IEEE Trans. Ind. Electron.*, vol. 61, no. 12, pp. 6852-6859, Dec. 2014.

[27] Y.-K. Kim, I. G. Jang, Y. Kim ; K.-S. Kim ; Soohyun Kim, "Structural Optimization of a Novel 6-DOF Pose Sensor System for Enhancing Noise Robustness at a Long Distance," *IEEE Trans. Ind. Electron.*, vol. 61, no. 10, pp. 5622-5631, Oct. 2014.

[28] S. Taghvaeeyan, R. Rajamani, "Two-Dimensional Sensor System for Automotive Crash Prediction," *IEEE Trans. Intel. Transp.*, vol. 15, no. 1, pp-178-190, Feb. 2014.

[29] C. Teuliere, E. Marchand, "A Dense and Direct Approach to Visual Servoing Using Depth Maps," *IEEE Trans. Robot.*, vol. 30, no. 5, pp. 1242-1249, Oct. 2014.

[30] S. Hoermann, P. Vinicius, K. Borges "Vehicle Localization and Classification Using Off-Board Vision and 3-D Models," *IEEE Trans. Robot.*, vol. 30, no. 2, pp. 432-447, Apr. 2014.

Samer S. Saab (SM'98) received his BS, MS and Ph.D. in Electrical Engineering in 1988, 1989 and 1992, respectively and an MA in Applied Mathematics in 1990, from the University of Pittsburgh. He joined the faculty of the Lebanese American University (LAU) in 1996. He is a Professor of Electrical Engineering at LAU. He served as the chairperson of the Electrical and Computer Engineering Department from 2005-2012 and Associate Dean of the School of Engineering at LAU from 2012 to 2013.

He worked for Union Switch and Signal and ABB Daimler-Benz Transportation, Pittsburgh, PA, 1993–1996. His research interests include multivariable control, iterative learning control, Kalman filtering, navigational positioning systems, and wireless communications.

Prof. Saab served on the Editorial Board of the IEEE TRANSACTIONS ON CONTROL SYSTEMS TECHNOLOGY from 2005 to 2011 and on the Editorial Board of the IEEE Control Systems Society-Conference from 2005 to 2009. He is currently serving on the Editorial Board of the IEEE TRANSACTIONS ON AUTOMATIC CONTROL. He is the recipient of the opening (2007–2008) LAU Best Research Award in engineering and physical sciences.

Hamze Msheik received a bachelor degree in computer systems engineering from Monash University Australia and M.S. degree in computer engineering from the Lebanese American University Lebanon, in 2009 and 2014 respectively. He worked as an RF research engineer at Monash University 2009-2011. He worked as a research engineer for RAMP 2011-2012. He is currently working as an RF engineer. His research interest are in the fields of RF design and robotics.